ELSEVIER

Polymer 44 (2003) 1151–1161

polymer

www.elsevier.com/locate/polymer

Preparation and properties of LDHs/polyimide nanocomposites

Huai-Bin Hsueh, Chuh-Yung Chen*

Department of Chemical Engineering, National Cheng-Kung University, Tainan 70101, Taiwan, ROC

Received 8 August 2002; received in revised form 18 November 2002; accepted 25 November 2002

Abstract

Layered double hydroxides/polyimide (LDHs/PI) nanocomposites were prepared from solution of polyamic acid (polyimide precursor) and LDH–amino benzoate using *N*,*N*-dimethylacetamide as a solvent. LDH–amino benzoate (LDH–AB) was obtained by coprecipitation method. The amino benzoate, grafted on the surface of the Mg/Al nanolayers, as a connector improved the compatibility between the inorganic Mg/Al nanolayers and the organic polyimide molecules. The dispersion behavior of Mg/Al nanolayers was investigated by transmission electron microscopy and X-ray diffraction, indicating that the Mg/Al nanolayers were exfoliated in PI matrix to form LDH–AB/PI nanocomposites. The maximum tensile strength and elongation of the LDH–AB/PI nanocomposites were found with the LDH–AB content of 5 and 4 wt%, respectively. The initial tensile modulus of these nanocomposites was increased with the LDH–AB content. These nanocomposites exhibited higher storage and loss moduli compared to those of pure PI. T_g of these nanocomposites increased with the LDH–AB content. Coefficients of thermal expansion (CTE, below and above T_g) of these nanocomposites deceased with the LDH–AB content. The thermal properties of these nanocomposites were enhanced by the incorporation of Mg/Al nanolayers in PI matrix.

Keywords: Polyimide; Layered double hydroxides (LDHs); Nanocomposites

1. Introduction

Aromatic polyimides are considered to be one of the most useful super-engineering plastics because of their outstanding dielectric, thermal, and mechanical properties at elevated temperatures [1]. The two-step method is a well-developed method for preparing polyimides. The method involves the preparation of polyamic acids (PAA) from diamines and dianhydrides in a polar solvent as the first step, followed by thermal imidization is proceeded to obtain polyimides (PI).

Inorganics/polymer nanocomposites are a class of composites in which the inorganic phase dimensions are in the order of nanometers [2–4]. These nanocomposites contain only a few percent of well-dispersed inorganic components of nanometer size in an organic polymer, and exhibit better properties than pure polymers [5–11]. The inorganic and organic phases are quite incompatible, resulting in phase separation. Thus, interfacial adhesion is introduced between the inorganic and organic components to minimize the degree of phase separation [12,13]. Generally, the existence of interfacial bonding, especially covalent bonding, between the inorganic and organic phases dramatically improves the mechanical properties such as modulus, tensile strength, hardness, fatigue, cracking, and resistance to corrosion [14–16]. Therefore, the surface of the inorganic components is organo-modified before the inorganics/polymer nanocomposites are prepared to enhance the compatibility between the inorganic and organic phases. Furthermore, the organo-modification makes the inorganic components more hydrophobic [17], enabling it to disperse in a polar solvent or polymer matrix. Therefore, the aggregated inorganic components will not form in the polymer matrix, and inorganics/polymer nanocomposites are formed. In sum, the organo-modification of the inorganic components is the most important process before the inorganics/polymer nanocomposites are prepared.

In recent years, many kinds of inorganics/polyimide nanocomposites have been studied [4,13,18–20]. These nanocomposites typically exhibited some properties superior to those of pure polyimide. Therefore, in order to improve the utility (e.g. thermal and mechanical properties) of PI in electronic industry, the field of design and creation

* Corresponding author. Tel.: +886-6-2757575-62643; fax: +886-6-2360464.
E-mail address: ccy7@ccmail.ncku.edu.tw (C.Y. Chen).

0032-3861/03/$ - see front matter © 2002 Elsevier Science Ltd. All rights reserved.
PII: S0032-3861(02)00887-X

of new construction inorganics/PI nanocomposites becomes more interesting.

Layered double hydroxides (LDHs) are a kind of layered materials that consists of positively charged layers and the interlayer exchangeable anions [21,22]. Their general composition can be represented as $[M(II)_{1-X}M(III)_X(OH)_2]^{X+}[A^{n-}_{X/n}\cdot m\,H_2O]^{X-}$, where M(II) and M(III) are divalent and trivalent cations, respectively, and A^{n-} is an exchangeable anion. In recent years, LDHs have received considerable attention because of their application as catalysts, ion exchangers, adsorbents, ceramic precursors, and organic–inorganic nanocomposites [23–29].

In the past 20 years, many reports about the intercalation of organic anions into LDHs have been published [30], but relatively few reports have discussed the incorporation of polymers into LDHs. Four major methods were used to prepare the LDHs/polymer nanocomposites: in situ polymerization, direct intercalation, restacking, and coprecipitation [31]. These studies on LDHs/polymer nanocomposites were mainly focused on intercalating the organic polymers into LDHs, but the application and performance of these LDHs/polymer nanocomposites have been relatively seldom reported.

LDHs/polyimides nanocomposites were never investigated in the past researches. In this study, the method of preparing LDHs/polyimide nanocomposites differs from that of conventional methods described above. The basic idea for producing the LDHs/polyimide nanocomposites is demonstrated as follows. The organo-modified LDHs are synthesized by incorporating organic anions into LDHs in the first step, followed by polymerization in the interlayer galleries of the LDHs. After the high molecular weight polymer is generated in the interlayer galleries, the stacking nanolayers of the LDHs lose their order, and then, the nanolayers are exfoliated to disperse in the polymer matrix. Thus, transparent and self-standing films of LDHs/polyimide nanocomposites are obtained. This study briefly discusses the preparation, characterization, and properties of the LDHs/PI nanocomposites.

2. Experimental

2.1. Materials

$Mg(NO_3)_2\cdot 6H_2O$, $Al(NO_3)_3\cdot 9H_2O$, and sodium hydroxide were used as supplied by Aldrich. 4-Amino benzoic acid was purchased from Riedel-deHaen and used without any purification. The doubly deionic water which had a conductivity of less than 0.4 $\mu S\ cm^{-1}$ at room temperature and a pH of ca. 6.47 was used to prepare the Mg/Al layered double hydroxides (Mg/Al LDHs). Pyromellitic anhydride (PMDA) was purchased from Criskev Company and purified from acetic anhydride. 4,4′-Oxydianiline (ODA) was purchased from Criskev Company and used without any purification. *N*,*N*-Dimethylacetamide (DMAc) was dried by distillation under reduced pressure over sodium hydride.

2.2. Preparation of Mg/Al LDH–amino benzoate (LDH–AB) and Mg/Al LDH–carbonate (LDH–CO_3^{2-})

The LDH–amino benzoate was prepared by the coprecipitation method. 0.8 g (0.02 mol) of NaOH was dissolved in 200 ml of deionic water, and then, 3.74 g (0.02 mol) of 4-amino benzoic acid was added to the sodium hydroxide solution. Magnesium nitrate, 5.12 g (0.02 mol) and aluminum nitrate, 3.75 g (0.01 mol) were dissolved in 50 ml of deionic water. The nitrate solution was then added dropwise to the vigorously stirred amino benzoate/NaOH solution at room temperature and the pH of the solution was maintained at 10 by the addition of 1 M of NaOH solution. After the addition of the nitrate solution, the mixture was reacted at 75 °C for 16 h. The slurry was then filtered until all the supernatant liquid had been removed. The sample was washed four times by doubly deionic water and dried at 70 °C. In order to minimize contamination with atmospheric CO_2, the preparation of the LDH–AB was under a nitrogen purge.

Coprecipitation method was used to prepare LDH–CO_3^{2-}, and LDH–CO_3^{2-} was prepared according to the method of Carlino and Hudson [32].

2.3. Preparation of PMDA/LDH–AB

LDH–AB, 1 g and 20 g of DMAc were poured into a flask and mixed at room temperature for 6 h under a nitrogen purge. PMDA, 0.5 g, was introduced into the flask and stirred with LDH–AB/DMAc mixtures at room temperature for 3 h. The mixtures were finally filtered and washed three times by 100 ml DMAc, respectively. The slurry was dried at 100 °C to obtain slightly yellow powder. Finally, PMDA/LDH–AB was obtained from the slightly yellow powder, which was treated by a thermal schedule as follows: 100 °C/2 h, 150 °C/2 h, 200 °C/2 h, 230 °C/3 h.

2.4. Preparation of LDH–AB/PI nanocomposites

Before preparing the LDH–AB/PI nanocomposites, the LDH–AB powder was well dispersed in DMAc under sonification for 6 h to obtain different concentrations of LDH–AB/DMAc solution. The different concentrations of LDH–AB/DMAc solution and 6 g (0.03 mol) of ODA were putted into a flask containing 40 g of DMAc under a nitrogen purge. After ODA was completely dissolved in DMAc, 12.41 g (0.0297 mol) of PMDA was added and the residual PMDA was washed into the flask by 40 g of DMAc. After the mixtures were stirred at room temperature for 3 h, the viscous LDH–AB/PAA solution was obtained. The viscous solutions were cast on glass plates. After drying in the air convection oven at 60 °C for 6 h, the imidization of LDH–AB/PAA films was proceeded by a thermal schedule as follows: 100,

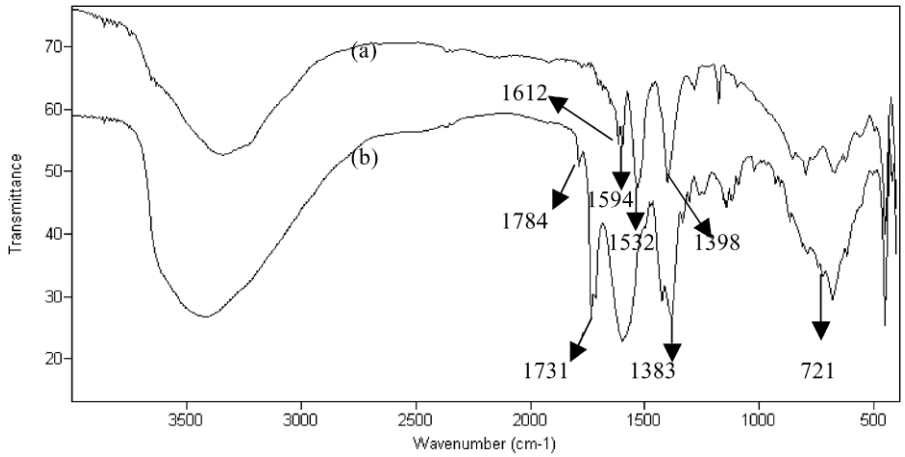

Fig. 1. The FT-IR spectrum of (a) LDH–AB and (b) PMDA/LDH–AB.

150, 200, 250, 300, and 350 °C for 1 h each to obtain the transparent LDH–AB/PI films. The LDH–AB contents compared to PI (ODA + PMDA) were 0, 0.5, 1, 2, 3, 5, 7, and 10 wt%.

2.5. Characterizations and measurements

The X-ray diffraction patterns were recorded on Rigaku RINT2000 X-ray Diffractometer, using Cu Kα radiation. FT-IR spectra were obtained with Bio-Rad FTS-40A FT-IR analysis. Carbon, hydrogen and nitrogen analyses were carried out with Heraeus CHN-O-RAPID Elemental Analyzer. Magnesium and aluminum analyses were carried out with HEWLETT PACKARD 4500 Inductively Coupled Plasma-Mass Spectrometer. Solid-state ^{27}Al NMR spectrum was obtained on a Bruker AVANCE 400 spectrometer. Microstructural characterizations of the nanocomposites were carried out using Hitachi HF-2000 FE TEM at an acceleration voltage of 200 kV. The tensile strength, elongation, and initial tensile modulus of the nanocomposites films were recorded on an Instron-4464 Universal Tester at a drawing rate of 5 mm/min. The dynamic mechanical analysis of the nanocomposites was carried out with Du-Pont 2980 Dynamic Mechanical Analyzer at a heating rate of 10 °C/min. The coefficients of linear thermal expansion of the nanocomposites films were obtained with Du-Pont 2940 Thermal Mechanical Analyzer at a heating rate of 10 °C/min under nitrogen purge. Dynamic thermogravimetric analysis (TGA) was performed with Perkin–Elmer TAC 7/DX at a heating rate of 20 °C/min under nitrogen purge. Isothermal TGA was carried out by Perkin–Elmer TAC 7/DX by heating the samples at 550 °C for 2.5 h.

3. Results and discussion

3.1. Characterization of LDH–AB

Fig. 1(a) shows the FT-IR spectrum of the LDH–AB. Strong absorption peaks of asymmetric and symmetric R–COO^- at 1532 and 1398 cm^{-1}, respectively, are observed. The characteristic peaks of the N–H bend and aromatic C=C stretching are at 1612 and 1594 cm^{-1}, respectively. These peaks demonstrate that amino benzoate was intercalated into the LDHs. A broad absorption peak between 3600 and 3000 cm^{-1} is assigned to O–H group stretches of both the hydroxide layers and the interlayer water.

Fig. 2 shows the ^{27}Al MAS NMR spectrum of the LDH–AB. Resonance of octahedrally coordinated aluminum within the brucite-like layers of the LDHs occurs in the range −10 to +20 ppm [32,33]. The ^{27}Al MAS NMR spectrum of the LDH–AB reveals a single resonance at +10 ppm, which indicates that all the aluminum atoms are octahedrally coordinated in the LDH–AB. Thus, the LDH–AB with brucite-like layers was successfully prepared.

ICP analysis for the LDH–AB yielded the following results: Al, 6.1% and Mg, 10.8%. C, H and N analysis yielded the following results: C, 22.3%, H, 4.77%, and N, 3.64%. The empirical formula of the LDH–AB, determined from the experimental data, is $Mg_6Al_{3.01}(OH)_{2.74}$(amino benzoate)$_{3.74}(CO_3^{2-})_{0.51}\cdot 7.91H_2O$, which perfectly correlates with the Mg/Al ratio (2:1) used to prepare the sample.

Fig. 3 shows the X-ray patterns of the LDH–CO_3^{2-} and

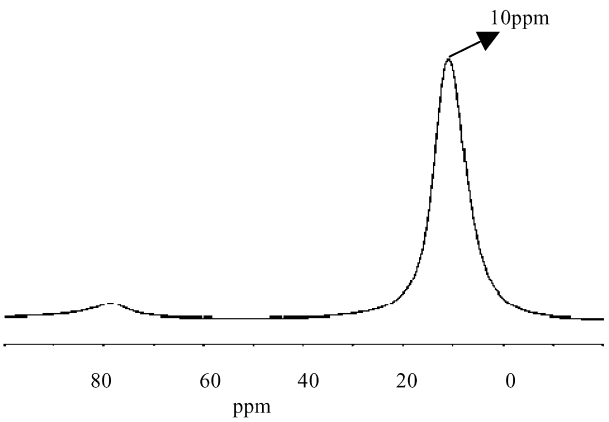

Fig. 2. ^{27}Al MAS NMR of LDH–AB.

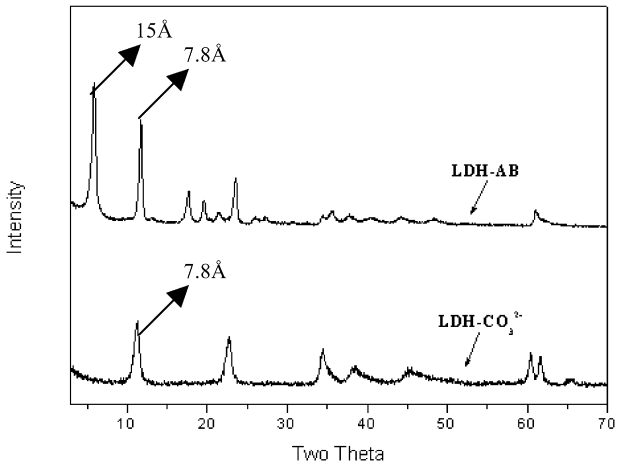

Fig. 3. The X-ray diffraction patterns of LDH–AB and LDH–CO_3^{2-}.

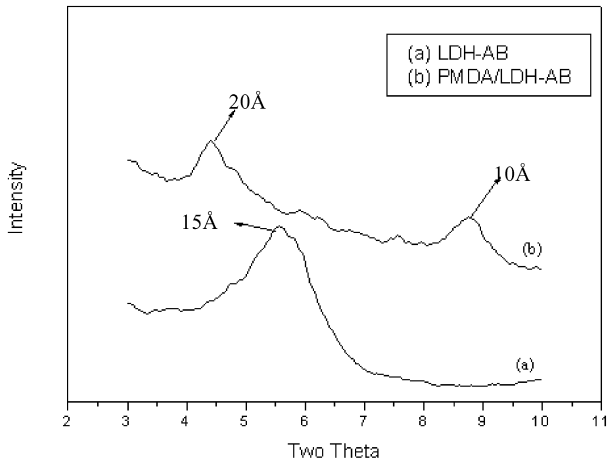

Fig. 4. The X-ray diffraction patterns of PMDA/LDH–AB and LDH–AB.

LDH–AB. The observed data show a basal spacing of 7.8 Å ($2\theta = 11.4°$) for the unintercalated LDH–CO_3^{2-}, increasing to 15 Å ($2\theta = 5.5°$) for the LDH–AB intercalated by amino benzoate anions. For the LDH–AB, an expanded structure is obtained and two peaks are present at $2\theta = 5.5°$ and $2\theta = 11.4°$, indicating that amino benzoate and carbonate are both present in the interlayer galleries of the LDH–AB.

From the results, not only the amino benzoate but also the carbonate are intercalated into LDHs, and the carbonate content is far less than the amino benzoate content. This finding perhaps follows from the involvement of less CO_2 molecules in the preparation of the LDH–AB powder.

Furthermore, a larger space between the Mg/Al nanolayers will promote the intercalation of a polymer, leading to easy exfoliation of the stacking Mg/Al nanolayers in polymer matrix to form LDHs/polymer nanocomposites.

3.2. Characterization of LDH–AB/PI nanocomposites

This study employed two-step procedure for manufacturing the LDH–AB/PI nanocomposites. The first was diffusion, whereby the polymerizable monomers of ODA and PMDA diffused with DMAc into the interlayer galleries of LDH–AB. The following step was polymerization. The polymerization of PAA from ODA and PMDA began from the amino benzoate on the surface of the Mg/Al nanolayers. Restated, after PMDA diffused into the interlayer galleries of LDH–AB, one anhydride functional group of PMDA reacted with amino benzoate and the other anhydride group of PMDA reacted with ODA. And then, PAA was polymerized in the interlayer galleries of LDH–AB to obtain LDH–AB/PAA nanocomposites. Therefore, the existence, or otherwise, of PMDA in the interlayer galleries is an important question to research. An additional experiment on PMDA/LDH–AB was performed to verify that the PMDA really diffused with DMAc into the interlayer galleries of the LDH–AB, and indeed reacted with the amine group of the amino benzoate. The X-ray diffraction curves in Fig. 4 show that the diffraction peaks of the PMDA/LDH–AB appear at $2\theta = 4.4°$ (d-spacing = 20 Å) and $2\theta = 8.8°$ (d-spacing = 10 Å). From the X-ray results of PMDA/LDH–AB, the space between the interlayer galleries increases to 20 Å and decreases to 10 Å, and thus differs from the original space in the LDH–AB. Scheme 1 presents the proposed model of changes in the interlayer space of the LDH–AB after PMDA was introduced. Fig. 1(b) shows the FT-IR spectrum of PMDA/LDH–AB, and the imide ring characteristic peaks are observed at 1784 (C=O asymmetric stretching), 1731 (C=O symmetric stretching), 1383 (C–N stretching), and 721 cm^{-1} (C=O bending). The X-ray patterns and FT-IR spectrum confirm that the PMDA molecules really diffused into the interlayer galleries to react with the amine group of the amino benzoate before the polymerization of PAA.

Fig. 5 plots the X-ray diffraction curves of LDH–AB/PI films with different LDH–AB contents. LDH–AB/PI films (1, 3, and 5 wt% LDH–AB contents) did not exhibit any diffraction peak at $2\theta = 3–10°$, whereas the LDH–AB powder yielded a diffraction peak at $2\theta = 7.8°$ (d-spacing = 11.4 Å). These results indicate that the Mg/Al nanolayers of LDH–AB were exfoliated and well dispersed

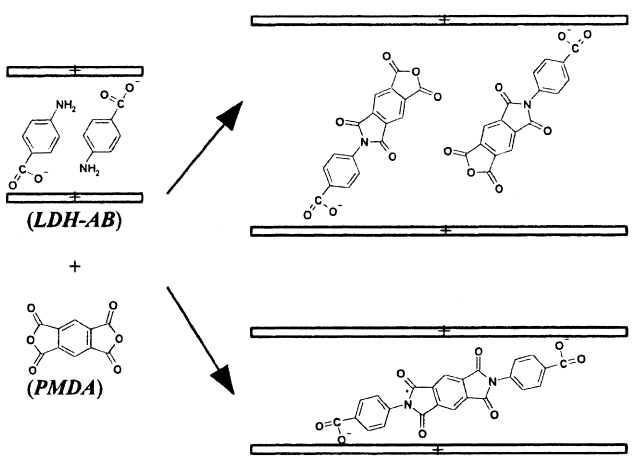

Scheme 1. Proposed model of the changes in the interlayer space of LDH–AB after PMDA was introduced.

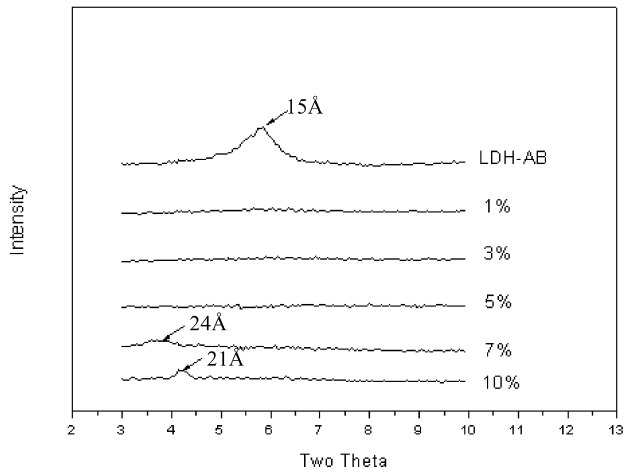

Fig. 5. The X-ray diffraction patterns of LDH–AB powder and LDH–AB/PI nanocomposites with various LDH–AB contents.

in the PI matrix. However, with 7 and 10 wt% LDH–AB contents, the LDH–AB/PI films produced a broad peak at $2\theta = 3.6°$ (d-spacing = 24 Å) and a sharp peak at $2\theta = 4.15°$ (d-spacing = 21 Å), respectively. These results suggest that a small amount of LDH–AB were not exfoliated but just intercalated.

Scheme 2 depicts the synthesis of LDH–AB/PI nanocomposites. After PMDA was added to the LDH–AB/ODA/DMAc solution, one anhydride functional group of PMDA reacted with the amine group of the amino benzoate and the other anhydride functional group reacted with ODA. Thus, the PAA was polymerized from the amino benzoate, and was grafted on the surface of the Mg/Al nanolayers. After a high molecular weight of PAA had been obtain in the interlayer galleries of the LDH–AB, the regularly structured stacking Mg/Al nanolayers were exfoliated by PAA. Then, the disordered LDH–AB nanolayers were well dispersed in a PAA matrix to form the LDH–AB/PAA nanocomposites. After the LDH–AB/PAA nanocomposites were imidizated, the LDH–AB/PI nanocomposites were obtained.

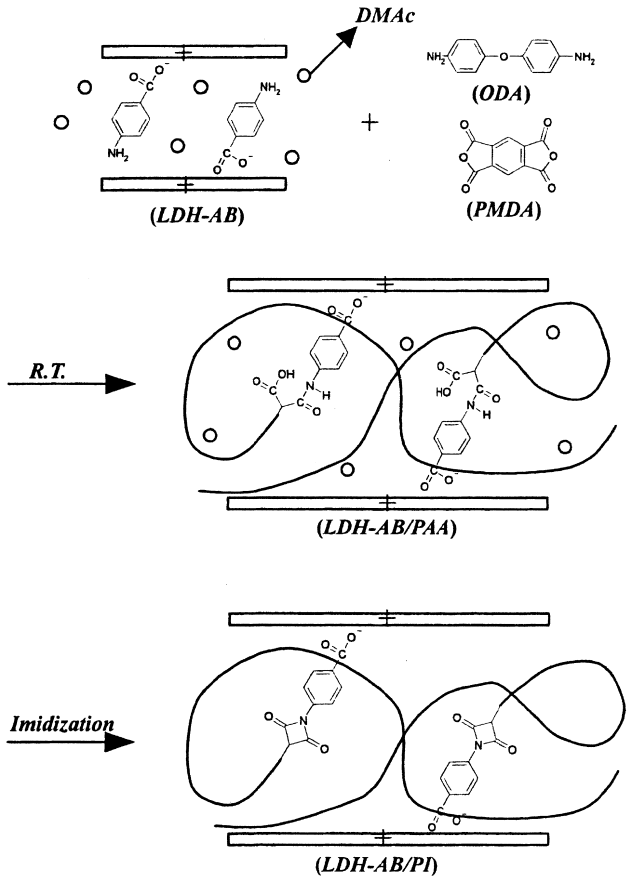

Scheme 2. The preparation of LDH–AB/PI nanocomposites.

The most direct measure of the dispersion of these Mg/Al nanolayers in PI matrix is typically TEM micrographs of the cross-sections of the LDH–AB/PI nanocomposites. Fig. 6(a) shows that the Mg/Al nanolayers were exfoliated and well dispersed in PI matrix in the case of LDH–AB/PI nanocomposites with 3 wt% LDH–AB. In Fig. 6(b)–(d), the fraction of the exfoliated nanolayers decreased and the fraction of the intercalated nanolayers increased as the LDH–AB content increased. With higher LDH–AB content, stacking Mg/Al nanolayers were not easily exfoliated but just intercalated. It was observed that the space between the intercalated nanolayers ranged from 2 to 10 nm. The difference spaces between the intercalated nanolayers can be explained that some PAA molecules were squeezed from the interlayer galleries during the removal of the solvent in imidization that reduced the space between the nanolayers. The probable reason for the smaller space (2–3 nm wide) between the intercalated nanolayers is that only the PMDA molecules or the PAA oligomers reacted with the amino benzoate in the interlayer galleries as the LDH–AB content increased, causing that the space between the nanolayers to be smaller than that intercalated by the PAA molecules with high molecular weight. Thus, the intercalated domains with smaller interlayer spaces (2–3 nm wide) are seemed to be aggregations of the Mg/Al nanolayers, representing a defect in the nanocomposites. Therefore, increasing the LDH–AB content leads to considerably poor properties of the LDH–AB/PI nanocomposites, due to the aggregation domains of the Mg/Al nanolayers. These results of TEM are consistent with the X-ray diffraction.

3.3. Tensile properties of LDH–AB/PI hybrid films

Fig. 7 plots typical stress–strain curves of LDH–AB/PI films with different LDH–AB contents. The tensile strength at break was observed to increase with the LDH–AB content. With 5 wt% LDH–AB content, the maximum tensile strength of the LDH–AB/PI nanocomposites was 131 MPa, which is 43% higher than pure PI. Generally, inorganic and organic phases are separated because they are incompatible, reducing the tensile strength of the inorganics/polymer nanocomposites. In this study, the amino benzoate, grafted

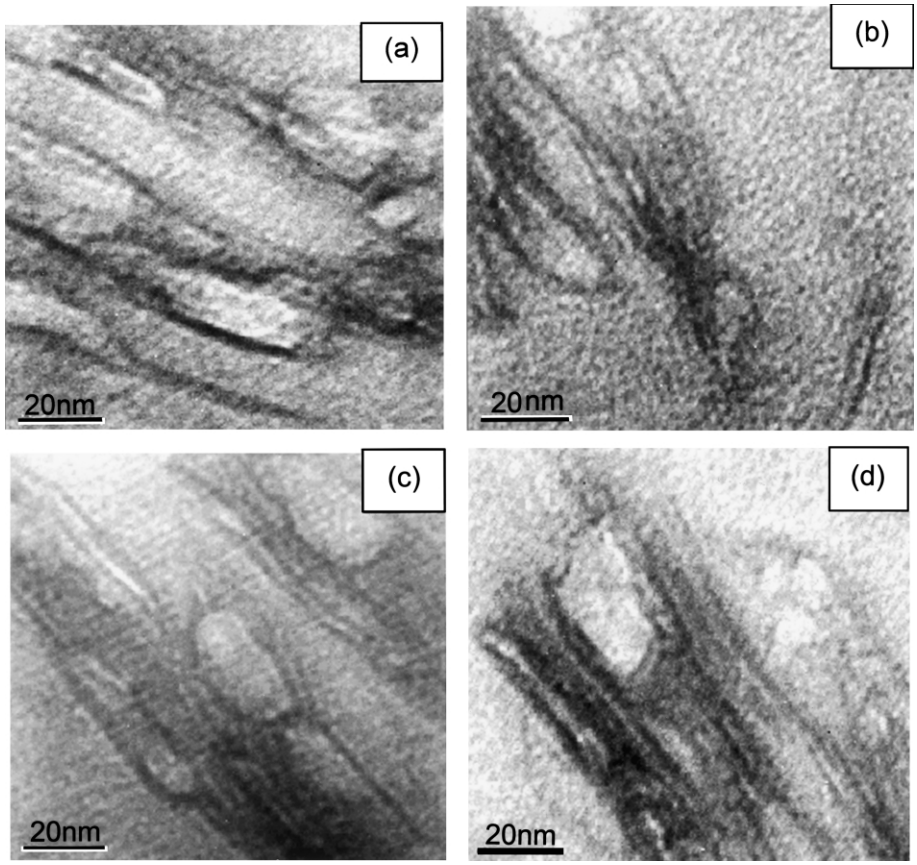

Fig. 6. TEM micrographs of LDH–AB/PI nanocomposites with various LDH–AB contents: (a) 3%, (b) 5%, (c) 7%, and (d) 10%.

on the surface of the Mg/Al nanolayers, is the connection between the Mg/Al nanolayers and the PI matrix, increasing the compatibility between these two phases. Thus, the well-dispersed Mg/Al nanolayers effectively enhance the tensile strength of the LDH–AB/PI nanocomposites. When the LDH–AB content exceeded 5 wt%, the tensile strength at break decreased but remained higher than that of pure PI, because a few amount of Mg/Al nanolayers were aggregated to form a defect in the nanocomposites, reducing tensile strength. Interestingly, the elongation of the LDH–AB/PI films increased with LDH–AB content. With 4 wt% LDH–AB content, the elongation at break was 35%, which is 63% higher than pure PI. By the same reasoning, the elongation behavior of the LDH–AB/PI nanocomposites is also determined by the interfacial bonding between the Mg/Al nanolayers and the PI matrix. However, when the LDH–AB content exceeded 4 wt%, the dramatically reduced strain was also determined that the PI molecules lack the infinity with the aggregation of the Mg/Al nanolayers.

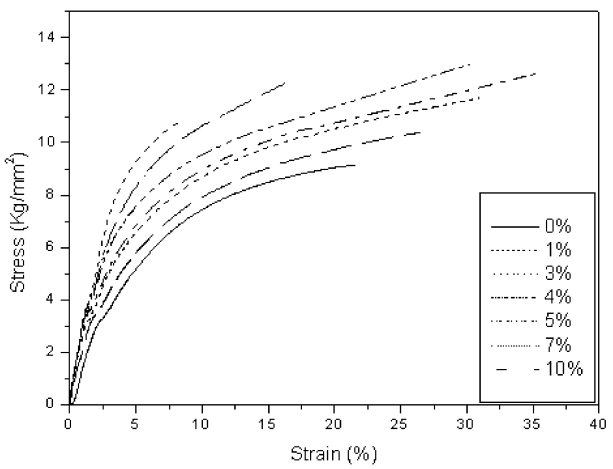

Fig. 7. Stress–strain curves of LDH–AB/PI films with various LDH–AB contents.

Fig. 7 also shows that the initial tensile modulus of the LDH–AB/PI nanocomposites increased with the LDH–AB content, because the stiffness of these nanocomposites was enhanced by the dispersion of rigid Mg/Al nanolayers in the PI matrix. The increase in the initial tensile modulus reflects the reinforcement on the LDH–AB/PI nanocomposites due to the dispersion of Mg/Al nanolayers in the PI matrix.

3.4. Viscoelastic properties of LDH–AB/PI nanocomposites

Figs. 8 and 9 show the temperature dependence of storage modulus (E') and loss modulus (E'') of the relevant nanocomposites. The storage modulus correlates with the elastic modulus of the materials, and the loss modulus is related with the energy lost due to the friction of polymer chain movement. Below the glass transition temperature,

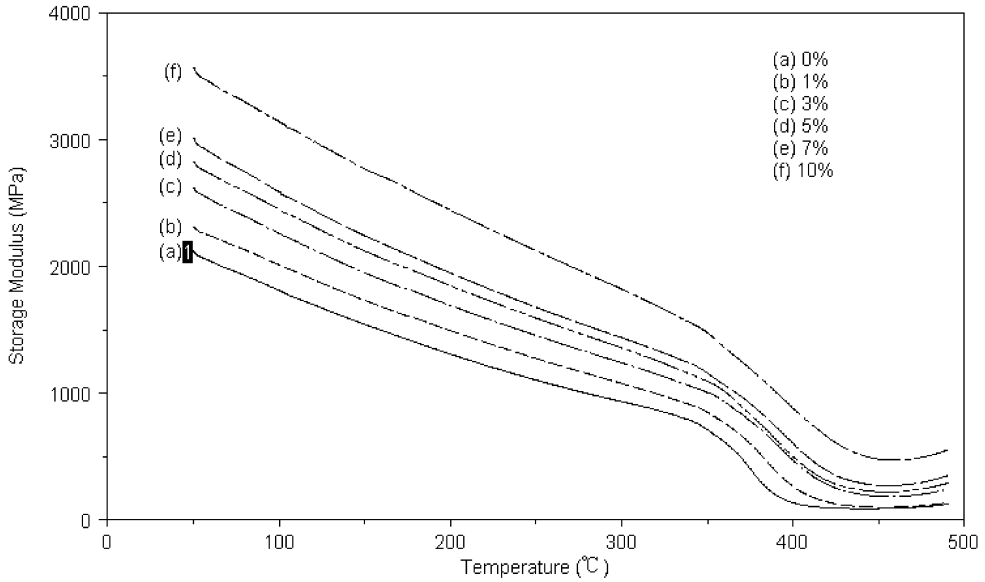

Fig. 8. Storage modulus, E', of the LDH–AB/PI nanocomposites with various LDH–AB contents.

the LDH–AB/PI nanocomposites were observed to exhibit a higher storage modulus than pure PI, and revealed a substantial drop in the storage modulus as the temperature increased. The storage modulus (around 50 °C) increased with the LDH–AB content because the stiffness of the LDH–AB/PI nanocomposites was enhanced by the introduction of the rigid Mg/Al nanolayers in PI matrix. The loss modulus (around 50 °C) of the LDH–AB/PI nanocomposites also slightly increased with the LDH–AB content. It can be explained that he friction between the Mg/Al nanolayers and the PI molecules increased as the PI chain moved as the temperature increased because of the thoroughly dispersed Mg/Al nanolayers in the PI matrix. The loss modulus increased accordingly. The results show that the LDH–AB/PI nanocomposites with Mg/Al nanolayers loading clearly had higher storage and loss moduli than did pure PI. Therefore, the excellent reinforcement effect of the Mg/Al nanolayers on the mechanical properties of LDH–AB/PI nanocomposites is again manifested.

T_g of the nanocomposites (from the maxima of E'' in Fig. 9) was confirmed to increase with the LDH–AB content. The higher T_g of the nanocomposites than that of the pure PI can be attributed to the more severe restriction of the PI chain mobility by the well-dispersed Mg/Al nanolayers, because the interaction between the Mg/Al nanolayers and PI molecules is strong.

Fig. 10 shows the temperature dependence of tan δ for the LDH–AB/PI nanocomposites. The loss factor tan δ is

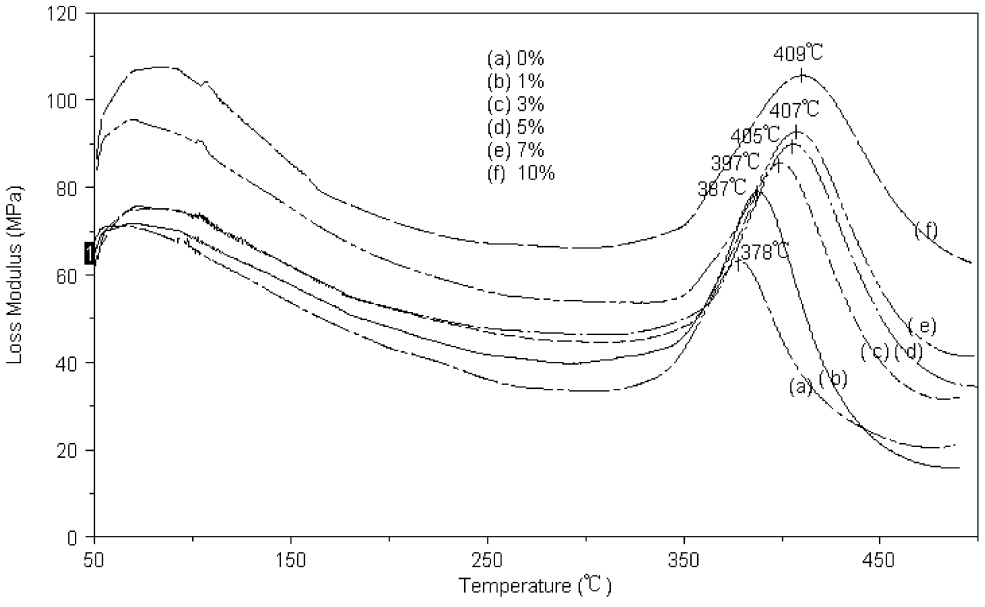

Fig. 9. Loss modulus, E'', of the LDH–AB/PI nanocomposites with various LDH–AB contents.

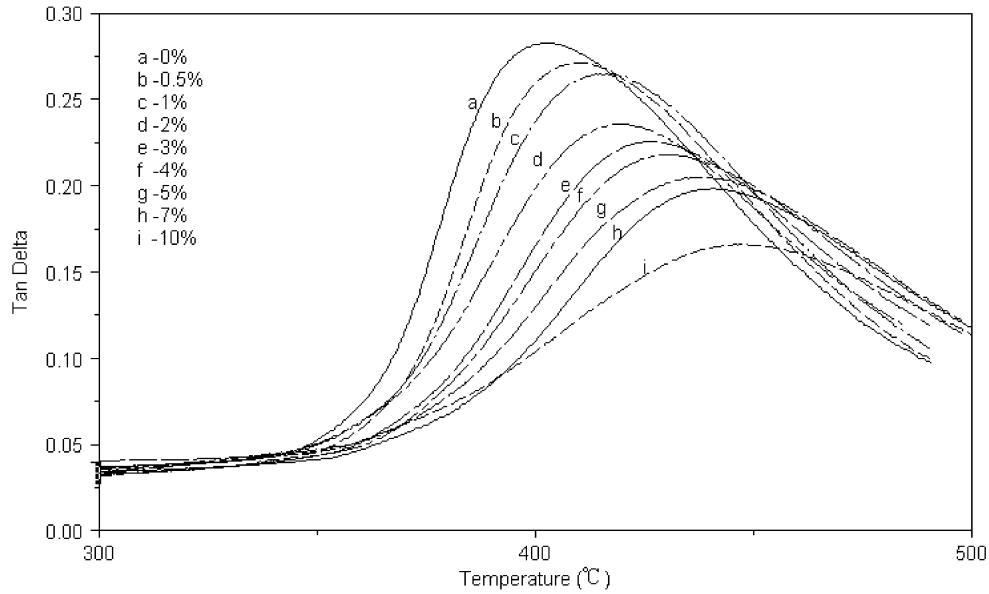

Fig. 10. tan δ of LDH–AB/PI nanocomposites with various LDH–AB contents.

calculated as the ratio of the loss modulus to the storage modulus (E''/E'), which is very sensitive to structural transformation of the materials. The tan δ peak values also determine T_g of the nanocomposites. T_g, obtained from maximum value of tan δ peak of these nanocomposites, shifted to a high temperature region by adding the LDH–AB to PI matrix because of the strength of the interaction between the Mg/Al nanolayers and PI molecules. Increasing the LDH–AB content also broadens and lowers the tan δ peak. The breadth of the tan δ peak is indicative of the relaxation of the polymer chain. The adhesion between the Mg/Al nanolayers and the PI molecules is such that the PI molecules that are tethered to the inorganic nanolayers exhibit more restrained chain mobility as the temperature increases and therefore their associated tan δ peak covers a wider temperature range. Thus, the breadth of the tan δ peak increases with LDH–AB content. The height of the tan δ peak is a measure of the energy damping characteristics of a material. The rigid Mg/Al nanolayers directly enhance the stiffness of the LDH–AB/PI nanocomposites because of the well-dispersed LDH–AB nanolayers in the PI matrix. The height of the tan δ peak thus decreases with LDH–AB content.

Fig. 11 shows the temperature dependence of the stiffness of these nanocomposites. The stiffness of the nanocomposites increased with the LDH–AB content, which resulted from the introduction of the rigid Mg/Al nanolayers into PI matrix.

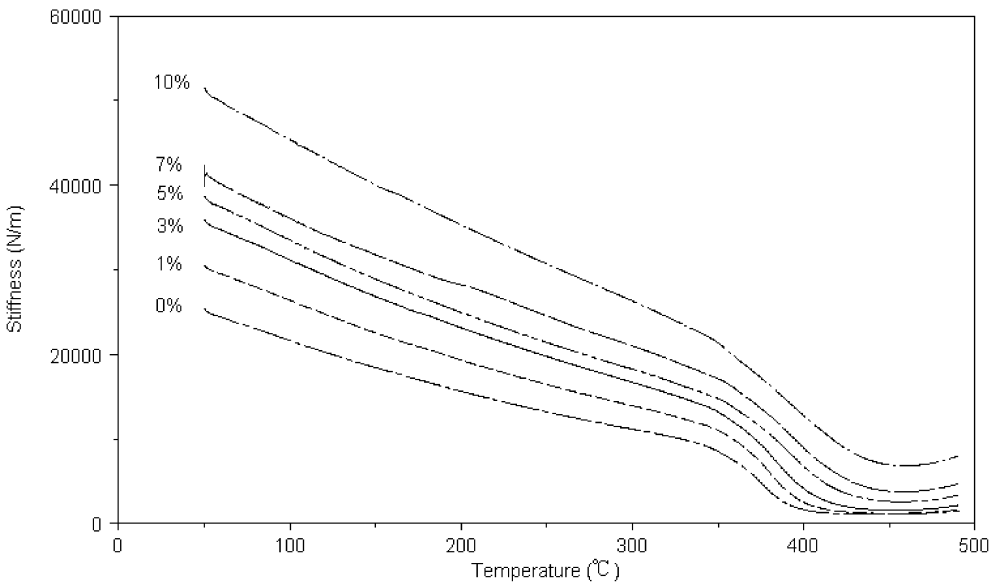

Fig. 11. Stiffness of LDH–AB/PI nanocomposites with various LDH–AB content.

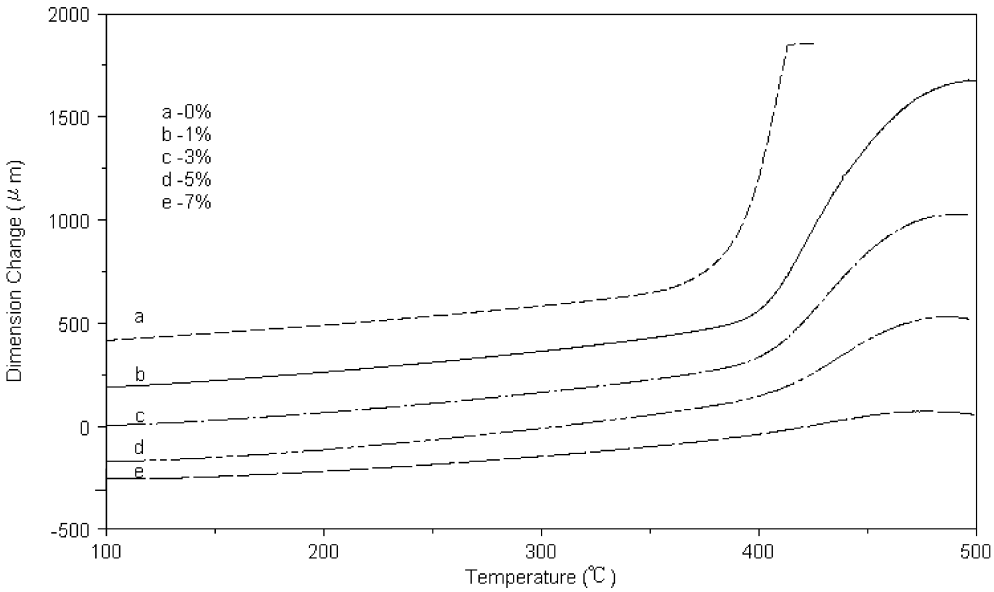

Fig. 12. Dimensional change–temperature of LDH–AB/PI nanocomposites with various LDH–AB contents.

The results described above show that the mechanical properties determined by tensile test and dynamic mechanical analysis substantially support the tendency that the mechanical properties of the LDH–AB/PI nanocomposites are enhanced with LDH–AB loading.

3.5. Coefficient of thermal expansion of LDH–AB/PI hybrid films

Fig. 12 shows the typical dimensional change versus temperature curves for LDH–AB/PI films. Fig. 13 shows coefficients of thermal expansion (CTE) and the reduced extent of CTE below and above T_g in the LDH–AB/PI films with different LDH–AB contents. CTE below and above T_g decreased as the LDH–AB content increased. It is worth noting that the reduced extent of CTE above T_g is more dramatic than that below T_g. These decreases in the CTE of the LDH–AB/PI nanocomposites, owing to the presence of the inorganic Mg/Al nanolayers can be explained as follows. Mg/Al nanolayers of the LDH–AB are more rigid than the PI molecules, and they neither deform nor relax like the PI molecules. Thus, given the excellent compatibility between the well-dispersed Mg/Al nanolayers and the PI molecules, the Mg/Al nanolayers effectively retard the thermal expansion of the PI molecules upon heating. Restated, the stiffness of the LDH–AB/PI nanocomposites was enhanced by the presence of rigid Mg/Al nanolayers that were well dispersed in PI matrix. Therefore, the CTE of the nanocomposites decreased as the LDH–AB content increased.

Fig. 14 shows the relationship between the onset glass transition temperature of the LDH–AB/PI nanocomposites and the LDH–AB content. T_g of the LDH–AB/PI nanocomposites increased with the LDH–AB content. This result can be explained that T_g of these nanocomposites increase mainly because the motion of the polymer chain is

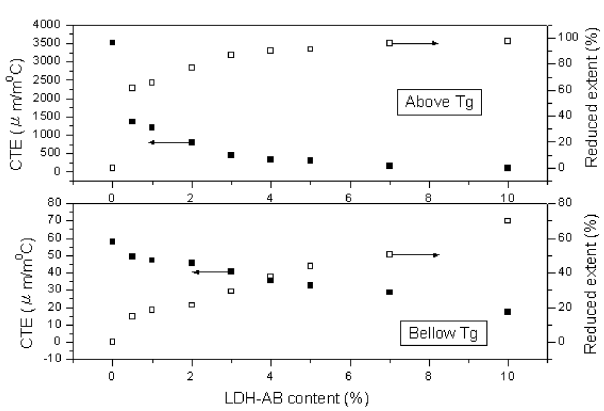

Fig. 13. Effect of LDH–AB content on the CTE and reduced extent of CTE of LDH–AB/PI nanocomposites.

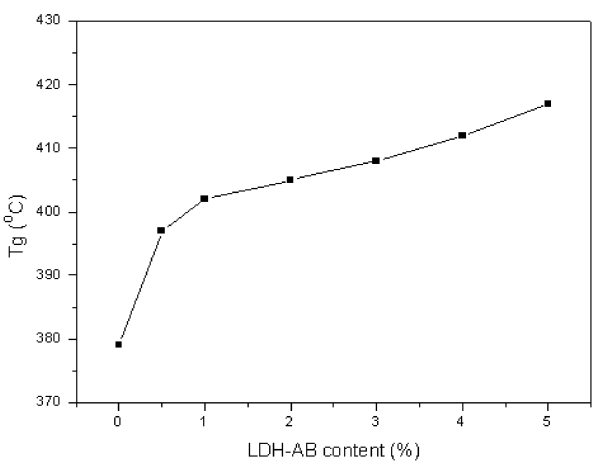

Fig. 14. Effect of LDH–AB content on the T_g from the onset temperature of TMA curves of LDH–AB/PI nanocomposites.

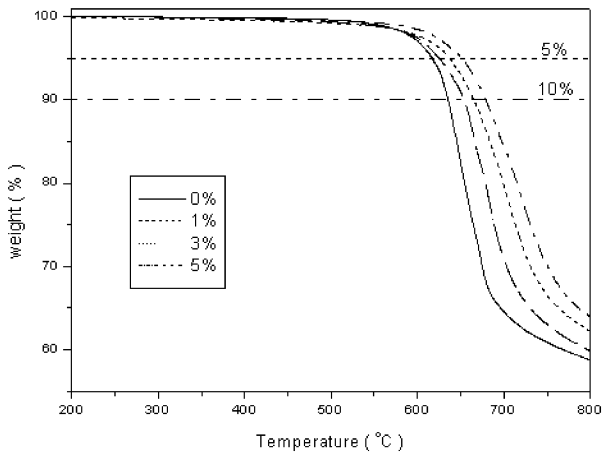

Fig. 15. TGA curves of LDH–AB/PI nanocomposites with various LDH–AB contents.

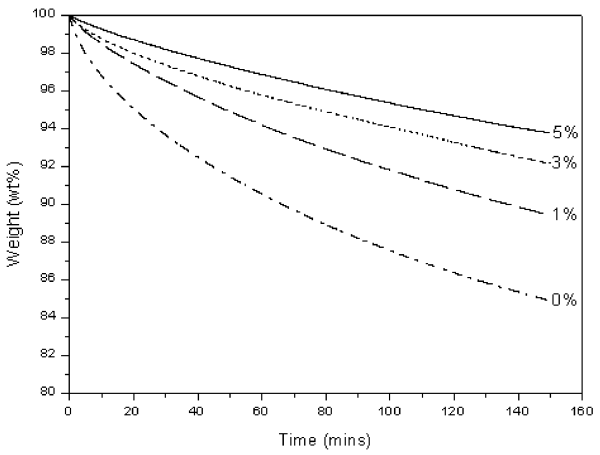

Fig. 17. Isothermal TGA curves of LDH–AB/PI nanocomposites with various LDH–AB contents at 550 ℃ for 2.5 h.

restricted by the inorganic Mg/Al nanolayers, since the adhesion between the nanolayers and PI molecules is strong. The tendency of T_g from TMA is consistent with that from DMA.

3.6. Thermal properties of LDH–AB/PI nanocomposites

Fig. 15 plots dynamic thermogravimetric curves of LDH–AB/PI nanocomposites with different LDH–AB contents. Fig. 16 shows the effect of LDH–AB content on the thermal decomposition temperature at 5 and 10 wt% weight loss. These figures show that the decomposition temperatures of these nanocomposites increased with the LDH–AB content. The dispersion of the Mg/Al nanolayers in the PI matrix enhance the thermal resistance of the LDH–AB/PI nanocomposites because the inorganic Mg/Al nanolayers have much higher thermal resistance than the organic PI molecules. Above 5 wt% LDH–AB loading, the decomposition temperature of these nanocomposites almost kept constant, because fewer Mg/Al nanolayers were aggregated in the PI matrix. The increase in the decomposition temperature of the nanocomposites depends on the dispersion behavior of the inorganic nanolayers, so the decomposition temperature increases dramatically with well dispersion of Mg/Al nanolayers in PI matrix.

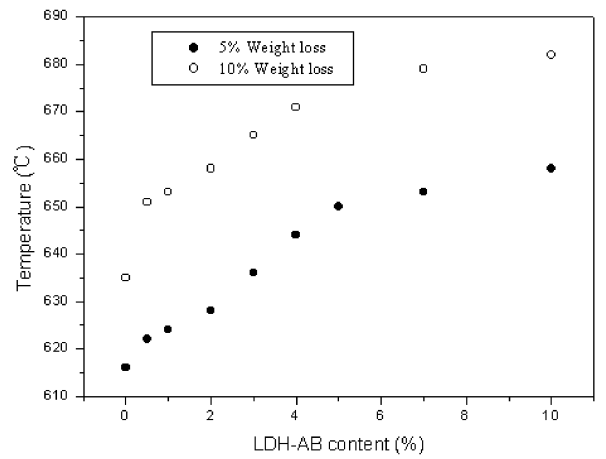

Fig. 16. Effect of LDH–AB content on the decomposition temperature at 5 and 10% weight loss of LDH–AB/PI nanocomposites.

Fig. 17 plots the isothermal thermogravimetric curves for LDH–AB/PI nanocomposites held at 550 ℃ for 2.5 h. The nanocomposites were observed to decompose more slowly than the pure PI. The initial decomposition of the aromatic polyimide is accompanied by the volatilization of carbon dioxide [34]. The LDH–AB nanolayers, well dispersed in the PI matrix, acted as a gas barrier, preventing volatile gas permeating out of the nanocomposites during the thermal treatment. Thus, the rate of decomposition of the LDH–AB/PI nanocomposites was lower than that of the pure PI because the thorough dispersion of the Mg/Al nanolayers increased the total length of the path of the volatile gas [18].

4. Conclusions

LDH–AB/PI nanocomposites were successfully prepared by the incorporation of LDH–AB in PI matrix. The Mg/Al nanolayers of the LDH–AB were exfoliated by PI molecules and well dispersed in PI matrix. Moreover, the amino benzoate, grafted on the surface of Mg/Al nanolayers, as a connector improved the compatibility between the inorganic Mg/Al nanolayers and organic PI molecules. Thus, these approaches dramatically improved the mechanical and thermal properties of the LDH–AB/PI nanocomposites as compared to pure PI.

References

[1] Mittal KL, Polyimides: synthesis characterization and application, vols. I and II. New York: Plenum Press; 1984.
[2] Kornmann X, Lindberg H, Berglund LA. Polymer 2001;42:1303.
[3] Pinnavaia TJ, Beall GW. Polymer–clay nanocomposites. New York: Wiley; 2000.

[4] Magaraphan R, Lilayuthalert W, Sirivat A, Schwank JW. Compos Sci Technol 2001;61:1253.
[5] Kojima Y, Usuki A, Kawasumi M, Okada A, Fukashima Y, Kurauchi T, Kamigaito O. J Mater Res 1993;8:1185.
[6] Okada A, Usuki A. Mater Sci Engng 1995;C3:109.
[7] Gilman JW. Appl Clay Sci 1999;15:31.
[8] Porter D, Metcalfe E, Thomas MJK. Fire Mater 2000;24:45.
[9] Yano K, Kojima Y, Usuki A, Okada A, Kurauchi T, Kamigaito O. J Polym Sci, Part A: Polym Chem 1993;21:2493.
[10] Lan T, Kaviratna PD, Pinnavaia TJ. Chem Mater 1994;6:573.
[11] Messersmith PB, Giannelis EP. J Polym Sci, Part A: Polym Chem 1995;33:1047.
[12] Chen Y, Iroh JO. Chem Mater 1999;11:1218.
[13] Mascia L, Kioul A. Polymer 1995;36:3649.
[14] Jang BZ. Compos Sci Technol 1992;44:333.
[15] Sohn JE. J Adhes 1985;19:15.
[16] Tien YI, Wei KH. Macromolecules 2001;34:9045.
[17] Tyan HL, Liu YC, Wei KH. Polymer 1999;40:4877.
[18] Agag T, Koga T, Takeichi T. Polymer 2001;42:3399.
[19] Tyan HL, Liu YC, Wei KH. Chem Mater 1999;11:1942.
[20] Kioul A, Mascia L. J Non-Cryst Solids 1994;175:169.
[21] Miyata S. Clays Clay Miner 1975;23:369.
[22] Ulibarri MA, Pavlovic I, Barriga C, Hermosin MC, Cornejo J. Appl Clay Sci 2001;18:17.
[23] Sels B, Vos DD, Buntinx M, Pierard F, Mesmaeker AK, Jacobs P. Nature 1999;400:855.
[24] Vaccari A. Catal Today 1998;41:53.
[25] Yun SK, Pinnavaia TJ. Chem Mater 1995;7:348.
[26] Moreyon JE, De Roy A, Forano C, Besse JP. Appl Clay Sci 1995;10:163.
[27] Pavan PC, Gomes G, Valim JB. Microporous Mesoporous Mater 1998;21:659.
[28] Hibino T, Tsunashima A. Chem Mater 1998;10:4055.
[29] Oriakhi CO, Farr IV, Lerner MM. J Mater Chem 1996;6:103.
[30] Carlino S. Solid State Ionics 1997;98:73.
[31] Leroux F, Besse JP. Chem Mater 2001;13:3507.
[32] Carlino S, Hudson MJ. J Mater Chem 1994;4:99.
[33] Carlino S, Hudson MJ, Husian SW, Knowles JA. Solid State Ionics 1996;84:117.
[34] Inagaki M, Takechi T, Hishiyama Y, Oberlin A. Chem Phys Carbon 1999;26:245.